RESEARCH ARTICLE | DECEMBER 17 2024

Shrimp structure as a test bed for ordinal pattern measures

Special Collection: From Sand to Shrimps: In Honor of Professor Jason A. C. Gallas

Yong Zou ; Norbert Marwan ; Xiujing Han; Reik V. Donner ; Jürgen Kurths

Chaos 34, 123154 (2024)
https://doi.org/10.1063/5.0238632

Chaos ARTICLE pubs.aip.org/aip/cha

Shrimp structure as a test bed for ordinal pattern measures

Cite as: Chaos 34, 123154 (2024); doi: 10.1063/5.0238632
Submitted: 13 September 2024 · Accepted: 27 November 2024 ·
Published Online: 17 December 2024

Yong Zou,[1,a)] Norbert Marwan,[2,3] Xiujing Han,[4] Reik V. Donner,[2,5] and Jürgen Kurths[2,6,7]

AFFILIATIONS

[1]School of Physics and Electronic Science, East China Normal University, Shanghai 200062, China
[2]Potsdam Institute for Climate Impact Research (PIK), Member of the Leibniz Association, Telegrafenberg A31, 14473 Potsdam, Germany
[3]Institute of Geosciences, University of Potsdam, Karl-Liebknecht-Str. 24–25, 14476 Potsdam, Germany
[4]Faculty of Civil Engineering and Mechanics, Jiangsu University, Zhenjiang 212013, China
[5]Department of Water, Environment, Construction and Safety, Magdeburg–Stendal University of Applied Sciences, Breitscheidstraße 2, 39114 Magdeburg, Germany
[6]Department of Physics, Humboldt University Berlin, Newtonstraße 15, 12489 Berlin, Germany
[7]Research Institute of Intelligent Complex Systems, Fudan University, 200433 Shanghai, China

Note: This paper is part of the Focus Issue, From Sand to Shrimps: In Honor of Professor Jason A. C. Gallas.
[a)]**Author to whom correspondence should be addressed:** yzou@phy.ecnu.edu.cn

ABSTRACT

Identifying complex periodic windows surrounded by chaos in the two or higher dimensional parameter space of certain dynamical systems is a challenging task for time series analysis based on complex network approaches. This holds particularly true for the case of shrimp structures, where different bifurcations occur when crossing different domain boundaries. The corresponding dynamics often exhibit either period-doubling when crossing the inner boundaries or, respectively, intermittency for outer boundaries. Numerically characterizing especially the period-doubling route to chaos is difficult for most existing complex network based time series analysis approaches. Here, we propose to use ordinal pattern transition networks (OPTNs) to characterize shrimp structures, making use of the fact that the transition behavior between ordinal patterns encodes additional dynamical information that is not captured by traditional ordinal measures such as permutation entropy. In particular, we compare three measures based on ordinal patterns: traditional permutation entropy ε_O, average amplitude fluctuations of ordinal patterns $\langle\sigma\rangle$, and OPTN out-link transition entropy ε_E. Our results demonstrate that among those three measures, ε_E performs best in distinguishing chaotic from periodic time series in terms of classification accuracy. Therefore, we conclude that transition frequencies between ordinal patterns encoded in the OPTN link weights provide complementary perspectives going beyond traditional methods of ordinal time series analysis that are solely based on pattern occurrence frequencies.

The ordinal pattern transition network (OPTN) approach offers an efficient method within the realm of complex network approaches for nonlinear time series analysis. An OPTN exploits successions of temporal variability patterns in time series, providing richer and more dynamic information beyond traditional ordinal pattern based measures like permutation entropy that are solely based on pattern occurrence frequencies alone. Here, we use the transition frequencies between subsequent ordinal patterns to characterize different bifurcation routes to chaos in the two-dimensional parameter space of certain complex systems. The corresponding new OPTN based ordinal measure exhibits very promising classification accuracy between periodic and chaotic dynamics. We therefore conclude that the OPTN approach provides a valuable tool for nonlinear time series analysis, offering a way to gain more reliable detail information about complex interwoven substructures in parameter space than traditional ordinal pattern based measures.

I. INTRODUCTION

Characterizing time series by means of complex network approaches is a recent and exciting development in nonlinear time series analysis.[1–7] Importantly, it offers novel ways to understand

hidden patterns and dynamics within time series data. The core concept hinges on transforming time series into a complex network representation. This is done by defining network nodes and edges based on certain entities (e.g., individual observations or patterns) within time series along with some relational criteria encoding selected aspects of the underlying dynamical variability.[6] Depending on the specific criteria underlying their definitions, there are several main classes of approaches including visibility graphs,[2,8] transition networks,[9] and proximity-based networks (like recurrence networks[3,4] or cycle networks[1]). Utilizing the corresponding transformations from time series into the complex network domain, we can quantify specific non-trivial time series properties by means of complex network characteristics, for example, clustering properties, centrality measures, or distributions of network motifs.[10] Thereby, network properties can reveal hidden relationships, recurrent patterns, and the overall dynamics of time series data.

Although complex network based time series analysis is promising, there are challenges including choices of methods and algorithmic parameter tuning for optimal results, which depend on the specific time series. For example, when constructing a recurrence network, the choice of embedding parameters and a proper distance threshold, which is used to determine whether or not two points are considered mutually recurrent and, hence, connected in the network, has been largely discussed in recent works.[6] When exploiting construction principles from the visibility graph family, the specific rule used to determine whether two points are visible to each other has pronounced effects on the resulting networks.[6,8]

In the present paper, we focus on the ordinal pattern transition network (OPTN) approach.[11,12] This method can be particularly useful when the computation of Lyapunov exponents or other traditional measures of nonlinear time series analysis becomes problematic due to the finite length of the available time series.[13] Unlike other time series network methods that explicitly use the actual data values, an OPTN is based on symbols characterizing the rank order of data point magnitudes within short sequences of a given length. This approach can be advantageous when the specific time series values are less important than their local tendencies, such as increasing or decreasing patterns. By encoding the likelihood of temporal successions (hereafter referred to as "transitions") of pairs of such ordinal patterns, an OPTN captures the temporal evolution of the time series, which can provide richer information compared to other network approaches.

The idea of OPTN has been largely motivated by the success of ordinal methods like the celebrated permutation entropy,[14,15] a technique within the broader field of symbolic dynamics analysis for time series.[16] Permutation entropy provides a single numerical value characterizing the complexity of the local ordering, which provides a static measure of randomness of the frequency distribution of ordinal patterns within the data. By contrast, the OPTN approach allows for a more detailed analysis of how the ordinal patterns evolve over time, which goes beyond just calculating a static permutation entropy. The OPTN approach has already shown promising results in applications to experimental time series across various fields, including electroencephalogram (EEG) data of brain activity,[7,12] electrocardiogram (ECG) based categorization of heartbeat patterns,[17] and climate and environmental data.[18,19] It is important to note, however, that the OPTN approach is still under further development, and its effectiveness can depend on the selection of its underlying parameters.

In traditional ordinal pattern analysis, embedding vectors with the same ordinal pattern can differ markedly from each other and exhibit large amplitude fluctuations. This can introduce substantial practical challenges and potentially affect the final results of ordinal and other types of time series analysis. For instance, large amplitude fluctuations can obscure ordinal patterns, since only the relative order of data point magnitudes is considered, which may show sensitivity to noise. In fact, the averaged amplitude fluctuations among trajectory segments characterized by the same ordinal patterns have been previously used to estimate the Kolmogorov–Sinai entropy.[20] We note that when dealing with large fluctuations, the choices of embedding dimension and time lag become even more critical than under noise-free conditions. Inappropriate parameter choices can amplify the effect of noise and thereby induce misleading network structures that are not representative for the underlying deterministic dynamical system.

Here, we particularly compare the respective performance of three quantitative ordinal measures, the traditional static permutation entropy, average amplitude fluctuations of ordinal patterns and out-link transition entropy of the corresponding OPTN, in characterizing dynamical transitions between chaos and periodic orbits in phase space. We specifically demonstrate the effectiveness of OPTN based measures by showing different boundary properties of so-called shrimp structures.

First reported by Jason Gallas,[21] shrimps arise in the two-dimensional parameter space of certain nonlinear systems. The corresponding structures exhibit curved, elongated shapes with a "head" and four thin "legs" branching outward. They represent regions in the parameter space, where the system shows periodic behavior, while the surrounding area is characterized by chaotic dynamics. In addition, a series of shrimp structures are aligned in a specific manner in the parameter space, showing fractal property.[22,23] The "legs" of different shrimps might be connected through intricate spirals, exhibiting different levels of organization, which however brings a big challenge to navigate through the parameter space and to control the dynamics when parameters are varied.[24,25] Shrimp structures have been observed in various nonlinear systems, including the sine-circle nontwist map,[26] economic models,[27] ecological multilayer networks,[28] a bio-chemical peroxidase–oxidase reaction system,[29] an epidemic spreading model,[30] a hydrodynamic model of a quantum dusty plasma,[31] and experiments with different electronic circuits.[32,33]

Understanding the types of bifurcation that occur when traversing different domain boundaries of a shrimp is crucial for predicting the system's behavior when we navigate in parameter space. Depending on the specific system and its governing equations, some common manifestations of complex behaviors around shrimps include period-doubling, intermittency, Hopf bifurcation, and others.[22] The specific bifurcation that occurs when crossing a boundary depends on the direction in which we cross it. Note that the "head" region of the shrimp can be a zone of high complexity with potentially mixed dynamics, which might be due to the convergence of different shrimps. Therefore, numerical methods are required to map out these boundaries and identify the associated

bifurcations, which show high potential for navigation and control as parameters of the system are varied.[22,34,35]

In this work, we propose using OPTN to characterize shrimp structures, which is motivated by the following considerations. From the viewpoint of methodology, we show that OPTN is a convenient and very helpful approach that captures complementary information beyond that exploited by other existing ordinal measures. Specifically, an OPTN focuses on the transition frequencies between ordinal patterns, which exhibit an enhanced sensitivity in characterizing different dynamics, e.g., distinguishing periodic from chaotic behavior, in comparison with previously introduced ordinal measures that are based on pattern occurrence frequencies only. From the viewpoint of application, OPTN excels at capturing transitions between states, making it useful for analyzing how the periodicity of the system changes when crossing shrimp structures.

The remainder of this paper is organized as follows: In Sec. II A, we introduce the basic ideas of ordinal patterns and the computation of permutation entropy. In Sec. II B, we discuss the computation of average amplitude fluctuations of ordinal patterns after showing that there are large fluctuations in the time series amplitudes among sequences corresponding to the same ordinal pattern. The concept of out-link transition entropy of an OPTN will be introduced in Sec. II C. We also discuss the effects of time series length, embedding dimension (Sec. II D), and additive noise (Sec. II E). Subsequently, we demonstrate the advantages of OPTN in characterizing bifurcation transitions in a one-dimensional parameter space (Sec. III) and across shrimps in two-dimensional parameter space (Sec. IV), where we focus on the classification accuracy of periodic and chaotic solutions by OPTN. In Sec. V, we give some conclusions.

II. THREE REPRESENTATIVE MEASURES OF ORDINAL PATTERN ANALYSIS

In this section, we will demonstrate the basic ideas of ordinal time series analysis and introduce three particular measures employed in this context in the course of the presented study. Since this work primarily addresses the numerical identification of shrimps, we will focus on a specific time-continuous dynamical system that is already known to exhibit the corresponding structures in its parameter space, the paradigmatic chaotic Rössler system

$$\left(\frac{dx}{dt}, \frac{dy}{dt}, \frac{dz}{dt}\right) = \left(-y - z,\ x + ay,\ b + z(x - c)\right). \tag{1}$$

In this system, the parameters a and b control the shape of the attractor, while c is often regarded as a single bifurcation parameter.

For illustrative purposes, we initially choose $a = b = 0.2$, $c = 5.7$. We integrate the system by a fourth-order Runge–Kutta integrator with a step size $h = 0.01$ and sample the trajectory every 20 steps, which leads to $\Delta t = 0.2$ between two consecutive time points. In what follows, we will first consider a time series of the x-variable with a length of $N = 10^5$ data points.

A. Ordinal patterns and permutation entropy

Let us start by reviewing briefly the basic ideas of ordinal pattern analysis,[14] which are further detailed in various reviewing articles.[36,37]

In the most traditional way of construction, ordinal patterns provide rank order representations of the embedding vectors in phase space. More specifically, for a scalar-valued (univariate) time series $\{x_k\}_{k=1}^{L}$ with $x_k = x(t_k)$ of L time points, we first reconstruct the phase space by time delay embedding,[13,38] i.e., we obtain a vector representation for the trajectory in phase space with individual embedding vectors,

$$\vec{x}_k = [x_k, x_{k+\tau}, \ldots, x_{k+(D-1)\tau}], \tag{2}$$

where D is called embedding dimension and τ embedding delay, which leads to $N = L - (D-1)\tau$ embedding vectors in this D-dimensional phase space. The effects of D and τ on the results of ordinal time series analysis will be qualitatively discussed below and, for the case of D, illustrated by numerical results in Sec. II D.

After having obtained the corresponding D-dimensional embedding, we derive the associated ordinal patterns to represent the corresponding embedding vectors, i.e., their rank vector as denoted by a symbol $\pi(t_k)$. There are totally $D!$ possible patterns. In the end, we get a symbolic representation $\{\pi(t_k)\}_{k=1,\ldots,N}$ (with $\pi \in \{\pi_1, \ldots, \pi_{D!}\}$) of the trajectory in phase space. It should be noted that equal values (ties) may have a significant impact on the ordinal representation and the associated statistics. In case they are rare, like in real measurements of high precision, we can either use the natural order of occurrence of equal values or introduce a small amount of noise to omit ties. However, if equal values occur too frequently in a signal, they may lead to significant effects which need to be carefully addressed.[39]

For a time series generated by a time-discrete map, a minimal time step of $\tau = 1$ provides a natural choice for the embedding delay. Two examples illustrating the ordinal properties of such maps will be briefly discussed in Appendices A and B, respectively. By contrast, for a time series resulting from a time-continuous dynamical system, like the Rössler system studied herein, the selection of the optimal embedding parameters, D and τ, is a crucial initial step in ordinal time series analysis. When exploiting other phase space based concepts of nonlinear time series analysis, such as fractal dimensions, D is often chosen at a value where the false nearest neighbors percentage drops below a certain threshold and τ is suggested by the first minimum of the average mutual information function or the first root of the auto-correlation function.[13] In the context of ordinal patterns, we however note that the value D determines the number of ordinal patterns in the resulting network. From the viewpoint of computation, we therefore suggest to experiment with different values of D while keeping in mind the possible convergence of ordinal measures for a given time series length N (see Sec. II D) and their associated computational cost. On the other hand, the choice of τ is particularly important for time series that are densely sampled from a time-continuous dynamical system. In such a situation, for a small τ, consecutive ordinal patterns can exhibit strong mutual dependency. It is hence important to choose an embedding delay τ that balances between capturing the system's fine-grained dynamics and minimizing redundancy and noise effects. Specifically, it is crucial to avoid choosing τ too large, as this can lead to a loss of fine-grained information. Therefore, we suggest to choose τ following the rules of thumb as discussed above, which precisely follow the same rationale. For the analysis of real

time series, we recommend to explore a range of D and τ values and evaluate the results using multiple criteria.

Once we have obtained an ordinal representation of a given univariate time series as described above, the corresponding permutation entropy ε_O is defined as the Shannon entropy of the distribution of ordinal patterns $P = \{p_{\pi_1}, p_{\pi_2}, \ldots, p_{\pi_{D!}}\}$,

$$\varepsilon_O = -\sum_{i=1}^{D!} p_{\pi_i} \log p_{\pi_i}. \tag{3}$$

In the case of a uniform distribution with the same relative frequency of all ordinal patterns, i.e., $P = \{1/D!, \ldots, 1/D!\}$, we obtain a maximum value of $\varepsilon_O = \log D!$.

B. Average amplitude fluctuations of ordinal patterns

In many examples, one observes that embedding vectors sharing the same ordinal patterns in phase space often show large amplitude variations (Fig. 1). This generically applies to any kind of time series from periodic, chaotic, and stochastic processes. In Appendix A, large amplitude variations of the same ordinal patterns are illustrated by time series of the chaotic logistic map. For the purpose of illustration, we obtain the ordinal representation for the time series of the x component of the Rössler system as described above by choosing the embedding parameters $D = 4$ and $\tau = 9$. In this case, we have in total 24 different ordinal patterns. We notice that the pattern $\pi_8 = (2, 1, 4, 3)$ shows the highest frequency among all patterns [Fig. 1(a)]. Different embedding vectors are represented by this same ordinal pattern π_8, which are highlighted in Fig. 1(b). Due to the determinism of the underlying system, some ordinal patterns are absent [Fig. 1(c)], which are referred to as missing or forbidden patterns. In the particular case of a time series of the logistic map, missing patterns are theoretically expected (see Fig. 15, Appendix A).

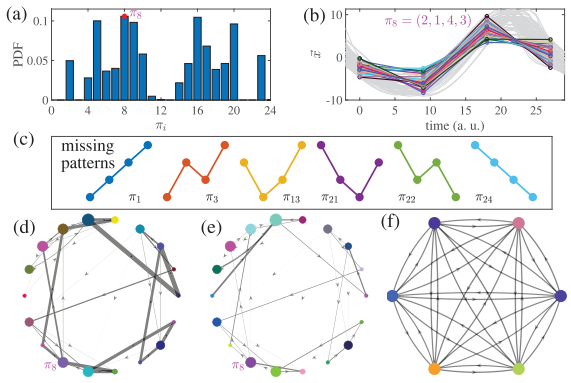

FIG. 1. Ordinal pattern frequencies and transition networks using the x-component of the Rössler system, $D = 4$, $\tau = 9$. (a) Frequencies of ordinal patterns, where pattern $\pi_8 = (2, 1, 4, 3)$ is highlighted. (b) Different embedding vectors sharing the same ordinal pattern. The gray background corresponds to trajectories showing the same ordinal pattern π_8. The time axis is shifted by arbitrary units to better show the ordering of the sampled points. (c) Missing ordinal patterns. (c) and (d) OPTN based on either (d) node-wise normalization or (e) globally normalized transition matrix. In both (d) and (e), missing pattern transitions are not shown to highlight the existing ones. For comparison, (f) shows a complete network generated from white noise ($D = 3$).

Notably, the amplitude fluctuations among trajectory segments characterized by the same ordinal patterns have been previously used for estimating the Kolmogorov–Sinai entropy quantitatively.[20] Taking up this idea, we first consider the standard deviation $\sigma_i(j)$ of the x variable in the jth component of the embedding vector. Then, we average $\sigma_i(j)$ over all components, which is denoted as $\langle\sigma\rangle$. It has been shown that the different scaling behavior of $\langle\sigma\rangle$ provides signatures which allow distinguishing deterministic from stochastic time series. More importantly, the logarithm of $\langle\sigma\rangle$ has been conjectured to provide a reliable estimate of the Kolmogorov–Sinai entropy.[20] Going even one step further, ordinal pattern positioned slopes have been recently proposed to characterize the fluctuations of ordinal patterns,[7] which have been successfully applied to distinguish between chaotic and stochastic dynamics.

C. OPTN out-link transition entropy

We note that in the two ordinal measures discussed above, the transition behavior between subsequent ordinal patterns has not yet been considered. Indeed, the latter aspect has only started being studied systematically along with the recent introduction of OPTN.[11,12,17] In this approach, each ordinal pattern is considered as a network node, and a directed and weighted link connecting two patterns in the network indicates the presence of the corresponding transition in the sequence of ordinal patterns derived from the original time series. Specifically, each link weight is given by the corresponding transition frequency $w_{ij} = p_{\pi_i \to \pi_j}$, i.e., the probability with which one specific ordinal pattern is followed by the other one.[11]

By considering all possible pairs of ordinal patterns, we obtain a transition matrix $\mathbf{W} = \{w_{ij}\}$ with $i, j \in \{1, \ldots, D!\}$. Based on $\mathbf{W}$, there are two slightly different ways to introduce normalizations. The first option has been proposed by McCullough *et al.*[12] and will be employed in the remainder of this work. More specifically, we consider the local out-link transition frequency from pattern π_i to π_j,

$$p_{\pi_i \to \pi_j} = \begin{cases} 0, & \text{if } \pi_i = \pi_j \\ \dfrac{w_{ij}}{\sum_{j, j \neq i} w_{ij}}, & \text{if } \pi_i \neq \pi_j. \end{cases} \tag{4}$$

Note that the transition frequency of Eq. (4) is row-wise normalized. The resulting network is shown in Fig. 1(d). Then, the out-link transition entropy for node π_i is computed as

$$\varepsilon_E^{\pi_i} = -\sum_{j=1, j \neq i}^{D!} p_{\pi_i \to \pi_j} \log p_{\pi_i \to \pi_j}, \tag{5}$$

and the out-link transition entropy of the network is defined as the (static) occurrence probability-weighted average over all ordinal patterns as

$$\varepsilon_E = \sum_{i=1}^{D!} p(\pi_i) \varepsilon_E^{\pi_i}. \tag{6}$$

In this way, ε_E captures the heterogeneous transition behavior of ordinal patterns, while considering the static occurrence frequencies of different patterns. Note that the row-wise normalization of Eq. (4) emphasizes the probability of transitioning from a specific ordinal pattern to another, which better captures the dynamics especially when the frequency of occurrence of different ordinal patterns varies significantly.

The second option is to use a global normalization,[5] which ensures that $\sum_{i,j}^{D!} w_{ij} = 1$, resulting in a globally normalized network transition entropy. One example network is shown in Fig. 1(e). The global normalization emphasizes the overall distribution of ordinal pattern transitions across the entire network, which might obscure the relative importance of transitions from a specific ordinal pattern. Therefore, we will not further consider this variant in what follows.

For the chaotic time series of the Rössler system whose OPTN representations are shown in Figs. 1(d) and 1(e), the transition frequencies are heterogeneously distributed. This can lead to the emergence of dominant pathways in the resulting network, where specific transitions between ordinal patterns occur more frequently than others. What is more, we observe the complete absence of certain links even between actually existing patterns, i.e., missing or forbidden transitions. This is not a statistical artifact due to the finite time series length, but rather a consequence of the deterministic nature of the Rössler system. By contrast, for an uncorrelated random time series, the transitions between ordinal patterns take place uniformly at random and hence lead to almost identical transition frequencies, i.e., showing less dominance of specific pathways compared to deterministic systems. Therefore, for white noise the resulting OPTN is a complete network with almost equal link weights as shown in Fig. 1(f).

Motivated by the concept of statistical complexity measures,[40–42] both ordinal permutation entropy and out-link transition entropy have been recently used for defining adjoint statistical complexity measures,[43] which quantify the distance of the empirical distribution (i.e., either P_{π_i} or $P_{\pi_i \to \pi_j}$) to a uniform distribution P_e. One of the advantages of out-link transition entropy is that it provides a pronounced distinction between different types of dynamical behaviors.[43] In principle, we could include any statistical complexity measure based on ordinal pattern transitions[43] in the presented analysis, which could further enrich the following discussion. However, we prefer here to keep it concise by using ε_E only.

D. Effects of time series length and embedding dimension

We use some example time series from the Rössler system to illustrate the effects of time series length and embedding dimension, which are two important parameters for ordinal pattern analysis. This discussion helps to fix the embedding dimension $D = 6$ and length $N = 10\,000$ in the later analysis.

The considered example time series include both periodic and chaotic trajectories. Periodic orbits of the Rössler system are characterized by the number of loops around the central point that occur before the loop series begins to repeat itself. Here, we include several periodic cases after period doubling bifurcation, i.e., period-2 ($c = 3$), period-4 ($c = 4.1$), and period-8 ($c = 4.15$) trajectories. In addition, we consider a chaotic case when $c = 5.7$. The other parameters are $a = b = 0.2$. These specific periodic examples will provide important insights that will later help us explaining the results for shrimps. The following results have been obtained by averaging over an ensemble of 100 realizations based on different initial conditions.

We first test the dependence of the ordinal measures on the length of time series while the embedding dimension $D = 6$ is kept fixed. We find that all three measures show a fast convergence to stable values when the length is increased (Fig. 2). Relatively large fluctuations are observed when $N < 10^4$. In general, larger values are obtained for chaotic time series than for periodic cases for all three measures ε_O, $\langle\sigma\rangle$, and ε_E. The average amplitude of fluctuations $\langle\sigma\rangle$ shows a relatively slow convergence for the chaotic series with values

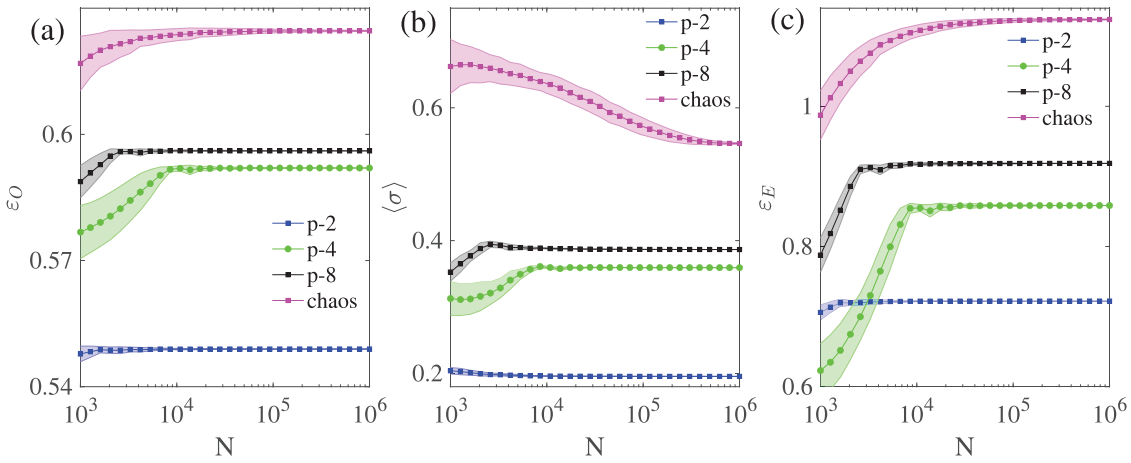

FIG. 2. Dependence of ordinal measures on the length of time series for a fixed $D = 6$. (a) ε_O, (b) $\langle\sigma\rangle$, and (c) ε_E. Example time series are from the Rössler system for different control parameter values c: $c = 3.0$ is for period-2 (blue), $c = 4.1$ for period-4 (green), $c = 4.15$ for period-8 (black), and $c = 5.7$ for chaotic time series (pink). Shaded areas correspond to standard deviations obtained using time series with 100 random initial conditions.

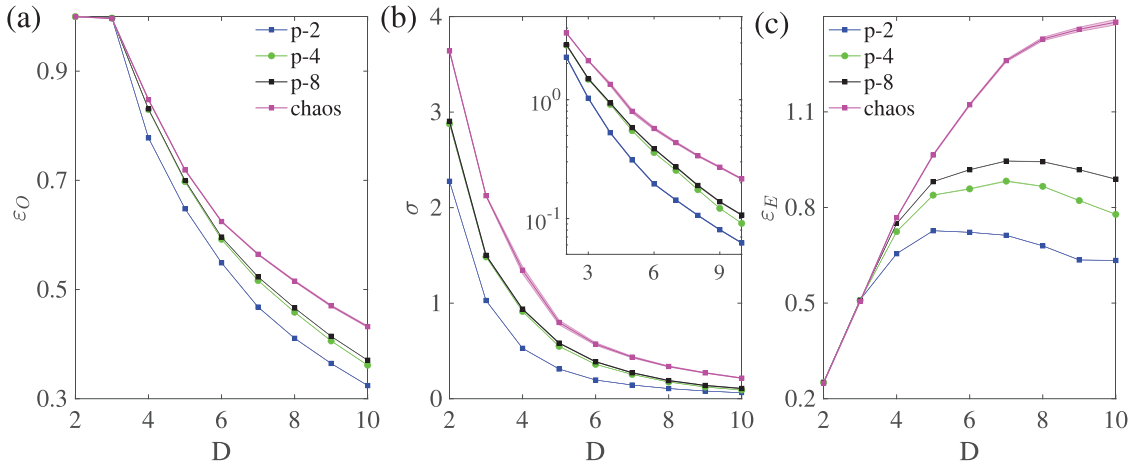

FIG. 3. Dependence of ordinal measures on the embedding dimension D for a fixed time series length $N = 10^5$. (a) ε_O, (b) $\langle\sigma\rangle$, and (c) ε_E. Example time series are the same as in Fig. 2. Shaded areas correspond to the standard deviations over 100 realizations of random initial conditions.

stabilizing only after $N \sim 10^5$ to 10^6 data points. In addition, comparing period-2 to period-8 time series, all measures increase as the period doubling bifurcation occurs. For small N ($N \lesssim 3000$), values of ε_E are larger for period-2 than for period-4, indicating a relatively slow convergence for the period-4 case.

Next, we study the dependence of the ordinal measures on the embedding dimension D for a fixed length $N = 10^5$ (Fig. 3). Again, ε_O of the chaotic time series has the largest values for all considered embedding dimensions D as compared to all periodic cases [Fig. 3(a)]. In addition, $\langle\sigma\rangle$ shows fast decays when D is increased. The logarithm of the average amplitude of fluctuations $\langle\sigma\rangle$ is expected to show a proper scaling[20] [see the inset in Fig. 3(b)]. In this case, we find that $\langle\sigma\rangle$ quickly converges to stable values when D increases. In addition, the disparity between chaotic and periodic time series is pronounced in the logarithmic scale only. However, for the out-link transition entropy ε_E, general increasing trends are observed for all time series when $D < 7$. Still, we get larger values for the chaotic series than for the periodic cases. We note that ε_E consistently shows a disparity between period-4 and period-8 time series [Fig. 3(c)], which, in turn, is not clearly observed in ε_O and $\langle\sigma\rangle$ [Figs. 3(a) and 3(b)].

Taking into account the convergence of the results (Fig. 2), we choose a fixed embedding dimension $D = 6$ and length $N = 10^4$ for the following analysis. Note that a larger value $D > 7$ is not recommended because it would significantly increase the computational cost of constructing and analyzing the OPTN. In addition, the data become sparse in a high-dimensional embedding space, which leads to difficulties in identifying meaningful patterns given a time series of finite length. Meanwhile, a high D may not be required for the original three-dimensional Rössler system.

E. Effects of observational noise

As a final step of this initial analysis, we demonstrate the robustness of the three ordinal measures when the input time series are contaminated by noise. In particular, we replace the x variable of the Rössler system by $\tilde{x}(t_k) = x(t_k) + \xi(t_k)$, where $\xi(t_k)$ is a random Gaussian white noise independent of $x(t_k)$. This noise term is referred to as observational noise since it represents possible random uncertainties during the measurement process. Specifically, the standard deviation σ_n of noise is taken proportional to the standard deviation of the input signal $x(t)$, i.e., $\sigma_n = \alpha\sigma_x$, where σ_x is the standard deviation of $x(t)$ and α represents the noise level.

Figure 4 shows that the values of all three ordinal measures generally increase when the noise level α is increased. From the viewpoint of visualization, ε_E in Fig. 4(c) shows relatively fast increasing trends since the OPTN captures the transition behavior between successive ordinal patterns. In any case, all three measures successfully distinguish chaotic time series from periodic signals at all observational noise levels α up to 20%.

III. ONE-PARAMETER BIFURCATION DIAGRAM

Ordinal measures show different capabilities in capturing bifurcation routes to chaos, since a chaotic system often generates different levels of chaos when parameters vary. In the case of the Rössler system, different levels of chaotic behavior include sparse chaos and filled-in chaos.[44,45] Therefore, we focus here on a period-doubling route to chaos, which exhibits period-3 windows.

Specifically, we choose $a = b = 0.1$ while c changes with a step size $\Delta c = 0.05$ in the interval $c \in [4, 18]$. The system is periodic for low values of c, but becomes chaotic when c is increased. Within this range of c-values, periodic windows are interspersed with chaotic intervals, and period-doubling occurs as c increases (Fig. 5). For example, the period-1 solution undergoes a period-doubling bifurcation at $c \approx 5.35$. This period-doubling bifurcation repeats at $c \approx 7.75$. A relatively large window with a period-3 orbit exists for $c \in [11.85, 12.45]$. Higher-period orbits are found, too, for example, period-5 at $c \approx 10.35$ and $c \approx 15.41$, period-6 at $c \approx 9.3$, and period-8 at $c \approx 14.85$. All these major periodic windows are captured by

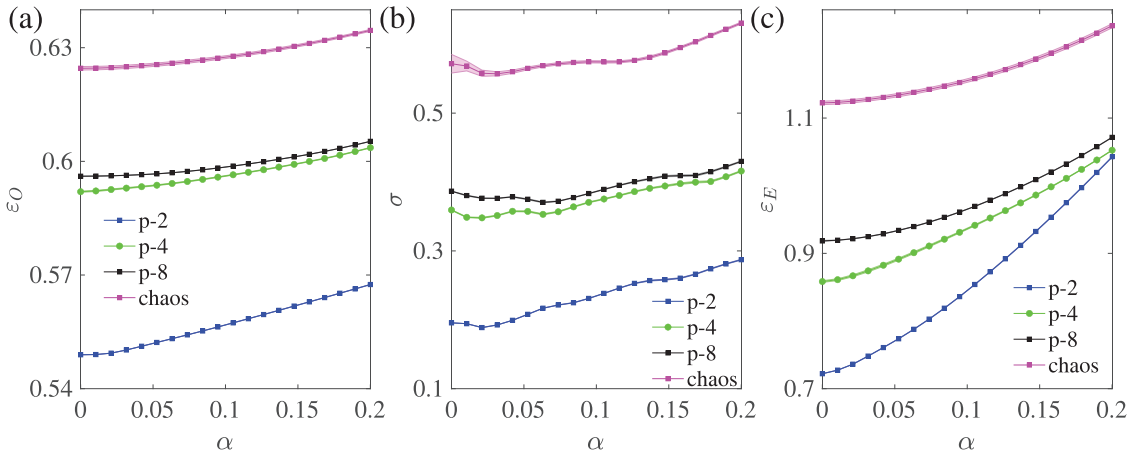

FIG. 4. Effects of different observational noise of levels $\alpha \in [0, 0.2]$ (time series length $N = 10^5$). (a) ε_O, (b) $\langle\sigma\rangle$, and (c) ε_E. Example time series are the same as in Fig. 2. Small fluctuations indicated by the shaded areas correspond to the standard deviations over 100 realizations of random initial conditions, and each time series is individually contaminated by 100 noise realizations for each noise level α.

the Lyapunov exponents $\lambda_{1,2}$ [highlighted by gray background in Fig. 5(b)].

Next, we characterize the different dynamics represented in the bifurcation diagram by the ordinal measures (Fig. 6). For each control parameter c, we integrate the equations 50 times using different random initial conditions. We then estimate the ordinal measures for all realizations and determine their mean values. All three ordinal measures, ε_O, $\langle\sigma\rangle$, and ε_E, basically capture the major low-period doubling windows, i.e., period-1 to period-2, period-2 to period-4, and the relatively large period-3 window. However, the small windows of higher periods are neither indicated convincingly by ε_O nor by $\langle\sigma\rangle$. By contrast, these higher-period windows are exclusively captured by ε_E.

It is interesting to note that the discrimination between periodic and chaotic windows of the Rössler system by means of all three ordinal measures improves significantly when the continuous time series of the x component is replaced by a discrete Poincaré map generated from the same coordinate (see Appendix B). This finding points to the fact that ordinal patterns provide a more natural description of time-discrete dynamics than of (artificially discretized) time-continuous one. Since the main scope of this work is the study of shrimp structures in time-continuous systems, we will not study this aspect further at this point.

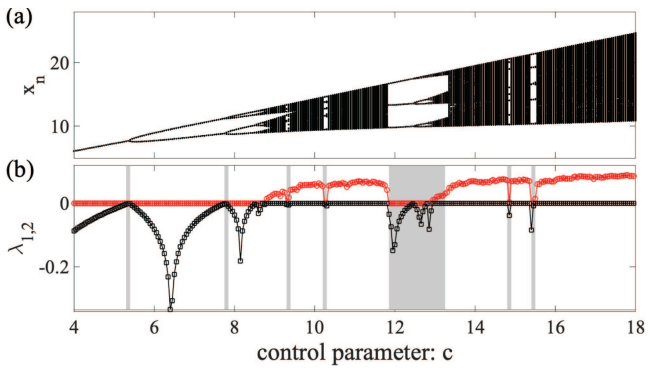

FIG. 5. One-parameter bifurcation diagram of the Rössler system when only the control parameter c is varied. (a) x_n on the Poincaré section $y = 0$, and (b) Lyapunov exponents $\lambda_{1,2}$, where several major periodic windows are highlighted by gray backgrounds.

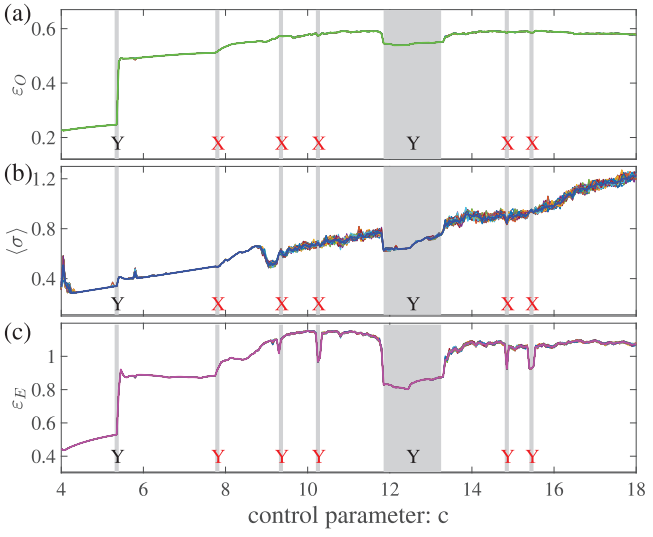

FIG. 6. Bifurcation diagram of the Rössler system as characterized by ordinal measures. (a) ε_O, (b) $\langle\sigma\rangle$, and (c) ε_O. Higher-period windows are captured by ε_E only as denoted with "Y," in contrast, neither by ε_O nor $\langle\sigma\rangle$ denoted with "X.".

IV. CHARACTERIZING SHRIMP STRUCTURES

A. Shrimp structures

In this section, we study the sensitivity of the ordinal measures in characterizing shrimp structures in the chaotic Rössler system when simultaneously varying two control parameters. Our previous computations based on recurrence analysis have already revealed the existence of complex intermingled periodic windows in the system.[46]

Here, we consider the two-dimensional parameter space of (c, a) and meanwhile choose $a = b$. The parameter regions of $(c, a) \in [20, 45] \times [0.2, 0.3]$ show complicate structures of the chaotic regime being interwoven with periodic windows. Following previous settings,[46] the parameter space of (c, a) is further divided into $n = 1000 \times 1000$ grid points, which results in the step size 0.0001 in $a \in [0.2, 0.3]$ and 0.025 in $c \in [20, 45]$. Numerical integration is carried out using a fourth-order Runge–Kutta integrator with a fixed step size of $h = 0.01$ time units and randomly chosen initial conditions. From those simulations, we obtain time series of 10^4 points with the sampling step $\Delta t = 0.2$ between two consecutive points after initial transients have been removed ($T_0 = 5000$). Again, we use only the x-variable of the system to obtain ordinal pattern representations and keep the same embedding parameters $D = 6$ and $\tau = 9$ for the entire parameter space.

The parameter space (c, a) color coded by the maximal Lyapunov exponent λ_1, the permutation entropy of ordinal patterns ε_O, the average amplitude fluctuations of ordinal patterns $\langle \sigma \rangle$, and the out-link transition entropy ε_E unveil characteristic patterns commonly associated with shrimp structures (Fig. 7). Note that λ_1 is shown here for comparison and statistical tests only, reproducing our previous computations in Zou *et al.*[46] Specifically, the maximum Lyapunov exponents have been estimated by integrating Eq. (1) sufficiently long until $t = 10\,000$, i.e., involving $N = 10\,000\,000$ data points with a sampling step corresponding to the considered integration step h. This means that the number of data points used for the evaluation of λ_1 is by a factor of 10^3 larger than for the ordinal measures, the reason being that stable estimates of Lyapunov exponents commonly require rather long time series.

The obtained results reproduce our previous findings gained from recurrence analysis,[46] demonstrating numerically that there are several well pronounced periodic regions embedded inside the chaotic regions. These periodic windows are of special importance, because they are aligned in a self-similar way. We find that all three ordinal measures are able to identify the corresponding shrimp structures. However, the discriminatory power of the individual measures for distinguishing between periodic and chaotic regions is clearly different, the further quantitative characterization of which will be the focus of the following analysis.

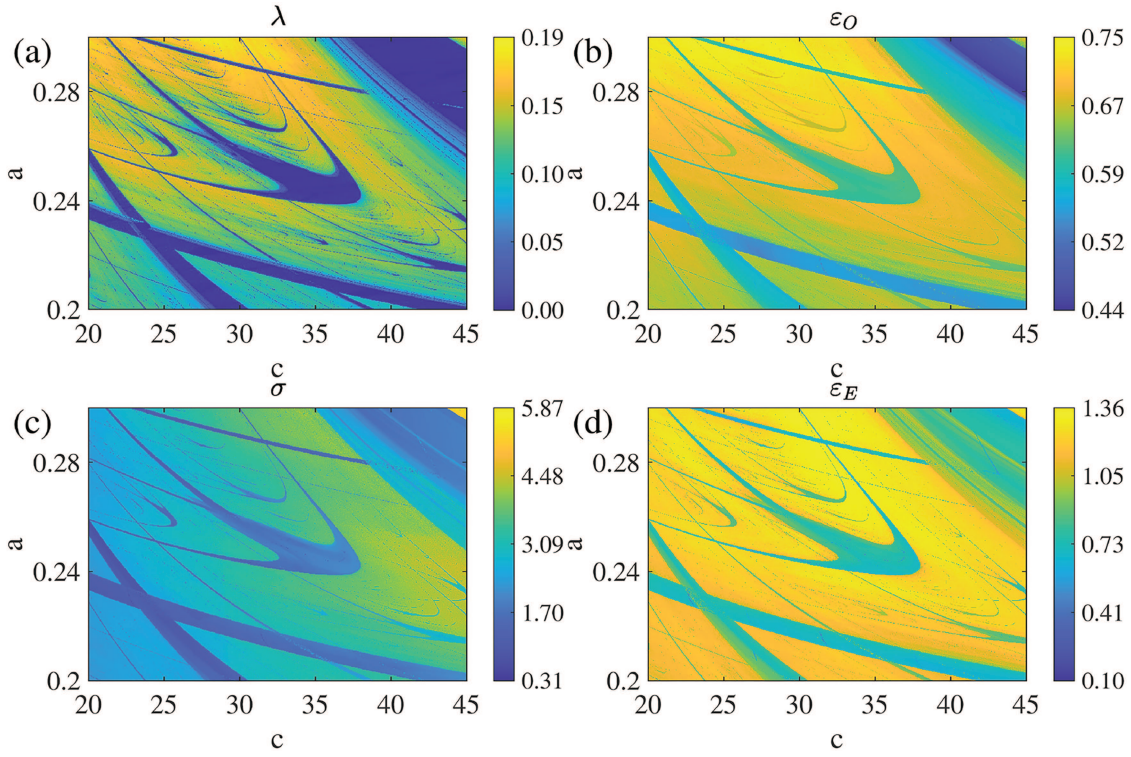

FIG. 7. Shrimp structures in the two-dimensional parameter space (c, a) of the Rössler system. (a) Maximal Lyapunov exponent λ_1, (b) static node permutation entropy ε_O, (c) average amplitude fluctuations of ordinal patterns $\langle \sigma \rangle$, and (d) dynamic node out-link entropy ε_E.

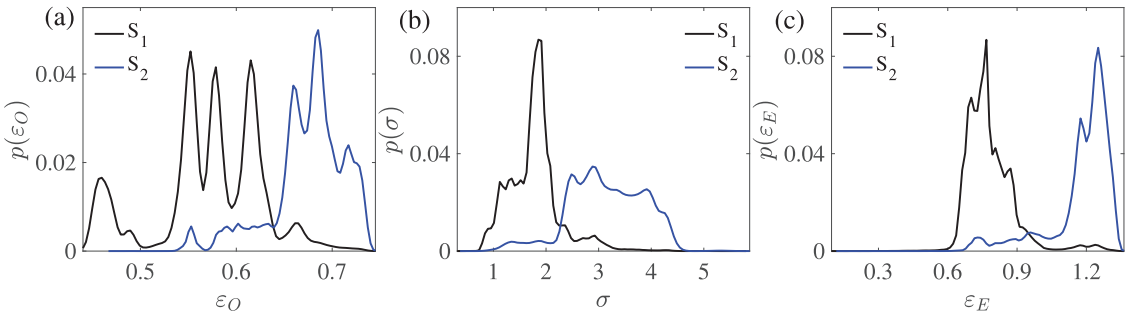

FIG. 8. Empirical estimates of probability distribution functions $p(\theta|S_i)$ of ordinal measures for parameter combinations (c, a) yielding $\lambda_1 \leq \lambda^*$ (S_1) and $\lambda_1 > \lambda^*$ (S_2), where $\lambda^* = 0.01$. (a) ε_O, (b) $\langle\sigma\rangle$, and (c) ε_E.

B. Statistical difference between periodic and chaotic cases

Due to the limited numerical precision, it is hard to distinguish weakly chaotic trajectories from periodic ones if λ_1 is close to zero. Indeed, there are numerous (c, a)-combinations leading to small positive values of λ_1 [Fig. 7(a)], which make the distinction difficult. Previously,[46] we proposed a supervised approach to statistically justify the discriminatory power of each measure with the help of a properly chosen λ_1, which will also be adopted in the following.

From a numerical point of view, we regard a time series as periodic if the numerical estimate of λ_1 is smaller than a predefined small threshold λ^*, say, $\lambda_1 \leq \lambda^*$. Accordingly, the entire (c, a) parameter plane is divided into two disjoint sets as

$$S_1(\lambda^*) := \{(c, a)|\lambda_1(c, a) \leq \lambda^*\}, \tag{7}$$

$$S_2(\lambda^*) := \{(c, a)|\lambda_1(c, a) > \lambda^*\}, \tag{8}$$

with group sizes n_1 and $n_2 = n - n_1$, respectively ($n = 1\,000\,000$ in our case). In other words, S_1 corresponds to parameter combinations with periodic trajectories, while S_2 contains the chaotic cases. We compare the frequencies of the different ordinal measures for S_1 and S_2 to evaluate their discrimination power (Fig. 8). Visually, all three measures show large values for S_2 of chaotic trajectories, however, exhibiting different levels of overlap with the smaller values for S_1. In addition, there are clear non-Gaussian multi-modal features for ε_O, which makes evaluating this statistics a little difficult. The case of ε_E gives the most similar shapes to Gaussian distributions.

In the next step, we characterize the accuracy of each ordinal measure for the binary classification task, quantifying the statistical distinction between the distributions $p(\theta|S_i)$ of the individual measures θ (where θ stands for ε_O, $\langle\sigma\rangle$, and ε_E, respectively) obtained for both S_1 and S_2 (Fig. 9). More specifically, we perform three statistical tests:

(i) The statistical difference between the distributions as shown in Fig. 8 is first assessed by a t test evaluating whether the group means are significantly different for various λ^*.
(ii) Since the underlying sample distributions are strongly non-Gaussian (Fig. 8), the t test is complemented by the Mann–Whitney U test.[47] In particular, we compute the value of the U statistic for testing against equality of the medians of two distributions, which is equivalent to an F test performed on the sets of rank numbers.
(iii) We numerically compute the overlap integral

$$\Psi = \int_{\min(\theta)}^{\max(\theta)} dx\, p(\theta|S_1)\, p(\theta|S_2), \tag{9}$$

which approximates the probability of classification errors by each ordinal measure θ for both groups (Fig. 8).

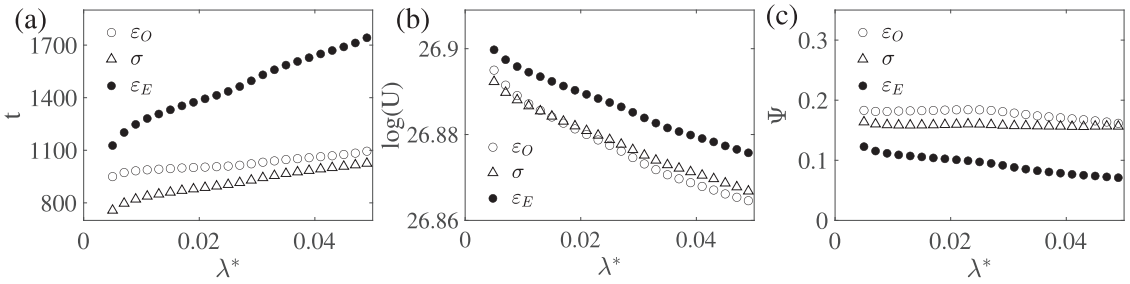

FIG. 9. Statistical tests for the difference between two sets S_1 and S_2, showing the discriminatory skills of the different measures ε_O, $\langle\sigma\rangle$, and ε_E. (a) t statistics, (b) U statistics (logarithmic scale), and (c) overlap integral Ψ.

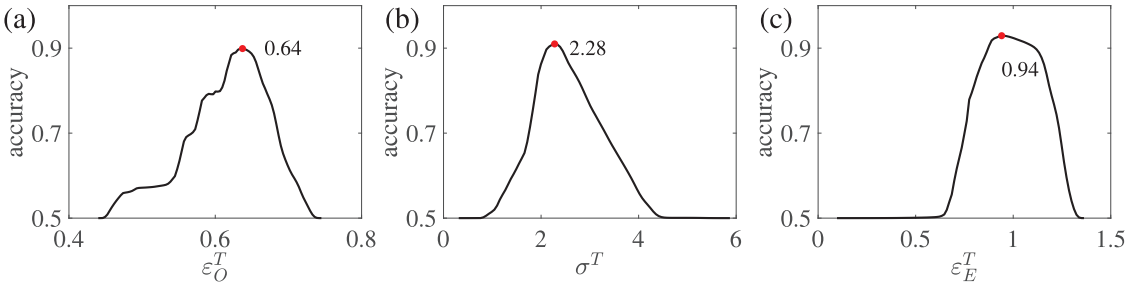

FIG. 10. Classification accuracy obtained by varying the discriminatory values of the ordinal measures in their respective entire range, where those individual thresholds θ^* are highlighted which provide the best classification. (a) ε_O, (b) $\langle\sigma\rangle$, and (c) ε_E.

For all $\lambda^* \in (0, 0.05)$, ε_E consistently yields the largest values of the statistics for both t and U test [Figs. 9(a) and 9(b)], which corresponds to the smallest overlap between the two distribution functions for S_1 and S_2 [Fig. 9(c)].

C. Classification accuracy

For a given λ^*, we compute the confusion matrix of each ordinal measure to characterize the classification accuracy by comparing the predicted results to the actual ones. The confusion matrix is widely used in classification tasks in machine learning, showing how many predictions are correct and incorrect per class, respectively, which helps in understanding the classes that are being confused by the ordinal measures. It computes the numbers of correctly classified true positive (TP) values and false positive (FP) values in the relevant class, the false negative (FN) cases in another class that should be in the relevant class, and the correctly classified true negative (TN) values in the other one.

More specifically, for a chosen λ^* [Eqs. (7) and (8)], we compare the reference labels (S_1, S_2) of the set of parameters (c, a) with another grouping (S_1', S_2') which is based on a variable threshold θ^* of the ordinal measure θ. Taking the periodic case as an example, the probabilities of correct as well as false detection of periodic behavior, $p_c^{(p)}$ and $p_f^{(p)}$, respectively, are given as

$$p_c^{(p)}(\lambda^*, \theta^*) = \left|S_1' \cap S_1\right| / \left|S_1\right|, \tag{10}$$

$$p_f^{(p)}(\lambda^*, \theta^*) = \left|S_1' \cap S_2\right| / \left|S_2\right|, \tag{11}$$

where $|S|$ represents the number of elements of the set S. In full analogy, we compute $p_c^{(c)}$ and $p_f^{(c)}$ for the chaotic trajectories. The overall performance accuracy of classification (ACC) as one of the most commonly used evaluation metrics in binary supervised classification problems is given by the following formula:[48]

$$\mathrm{ACC} = \frac{p_c^{(p)} + p_c^{(c)}}{p_c^{(p)} + p_f^{(p)} + p_f^{(c)} + p_c^{(c)}}. \tag{12}$$

It is easy to see that $\mathrm{ACC} \in [0.5, 1]$, where 0.5 represents a random classification.

In theory, we do not have a natural threshold θ^* for all ordinal measures to classify a given time series as either a periodic or chaotic one. A simple solution would be to study the classification accuracy ACC over full range of possible values of θ and then seek for the corresponding maximum (Fig. 10). We find that unlike for ε_O, the corresponding curves for both $\langle\sigma\rangle$ and ε_E are fairly smooth and have nearly-symmetric shapes with a single pronounced maximum. From the viewpoint of ordinal measures, the peak positions of Fig. 10 provide the best classification accuracy. Therefore, using the critical thresholds as suggested by Fig. 10, we calculate the success rates in the classification while λ_1^* is varied $\lambda_1^* \in (0, 0.05)$ [Fig. 11(a)]. As expected from our previous analyses above, the OPTN out-link transition entropy ε_E indeed provides the best classification rate compared to the other two ordinal measures.

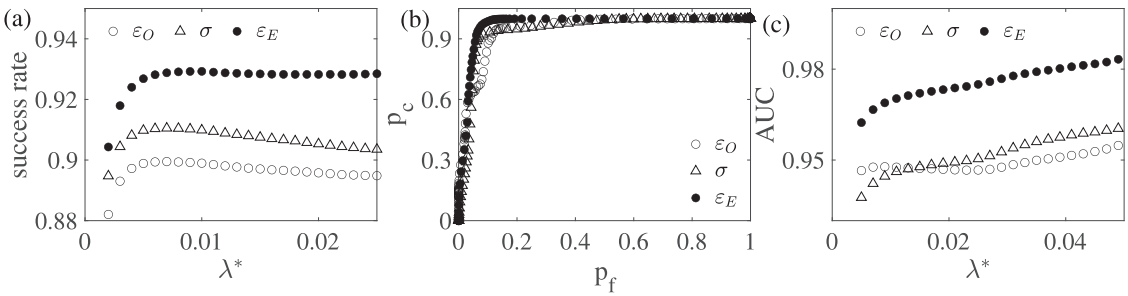

FIG. 11. (a) Success rates for different λ_1^*, (b) ROC curve for the periodic orbits for $\lambda^* = 0.01$, (c) area under the ROC curve (AUC) in dependence on λ_1 for the three considered ordinal measures. For $\lambda^* = 0.01$, AUC takes the values 0.948 (ε_O), 0.946 ($\langle\sigma\rangle$), and 0.97 (ε_E), respectively.

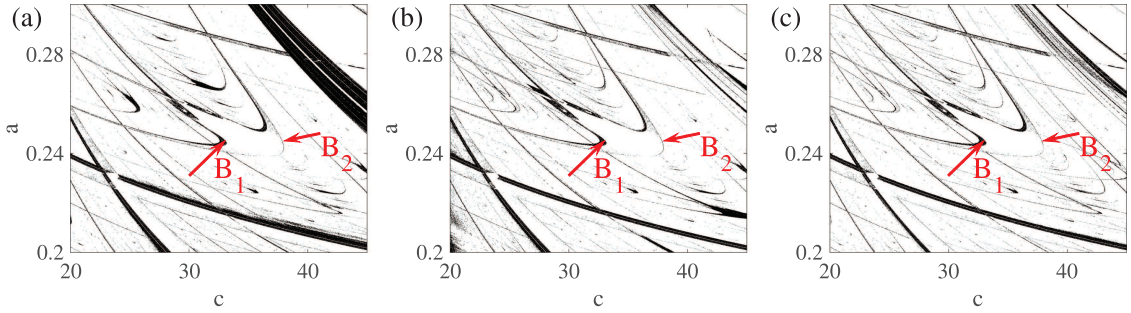

FIG. 12. Classification errors in the parameter space for the groupings S_1, S_2, S_1', and S_2' for $\lambda^* = 0.01$ when each measure shows the best success rates in classification. (a) ε_O, (b) $\langle\sigma\rangle$, and (c) ε_E.

When studying the correct as well as false detection rates only for periodic behavior, namely, only $p_c^{(p)}$ and $p_f^{(p)}$, we obtain a continuous curve as the discriminatory threshold θ^* is varied, which is known as the receiver operating characteristics (ROC) curve.[48] In particular, we vary θ^* over the full range of possible values with λ^* simultaneously being kept fixed [Fig. 11(b)]. The ROC curve shows the trade-off between a high probability of correct and a low probability of false detections of periodic behavior. In the ROC plot, the minimal distance to the upper left corner $(0, 1)$ suggests a possible best classification for a given $\lambda^* = 0.01$ [Fig. 11(b)]. In particular, we have $d^O_{\min} = 0.139$, $d^\sigma_{\min} = 0.113$, and $d^E_{\min} = 0.085$. In addition, the area under the ROC curve (AUC) is often used for quantitatively characterizing the classification performance of different measures.[48] In our case, AUC confirms that ε_E is the most successful statistics in classifying periodic and chaotic behavior in the entire (c, a) parameter plane of the Rössler system, while ε_O and $\langle\sigma\rangle$ show more or less the same, yet somewhat lower power [Fig. 11(c)]. Specifically, in this particular classification task, ε_E outperforms the previously studied recurrence network measures, among which the best classifiers exhibit AUC values of about 0.94.[46]

D. Reasons of classification errors

Classification errors appear mainly along the domain boundaries, when the system generates bifurcations from periodic to chaotic dynamics (Fig. 12). In addition, the system produces either period-doubling (B_1 regions in Fig. 12) or intermittency (B_2 regions).[21,23] All ordinal measures show a classification sensitivity across the intermittency bifurcations, however remain to be blurred in the period-doubling region. When the system generates period doubling routes to chaos, relatively large fluctuations are observed due to the finite time series length for all three ordinal measures (Fig. 2). Indeed, the Rössler system shows weak sparse chaos resulting from the period-doubling, with the corresponding chaotic attractor exhibiting much geometric similarity with the neighboring higher-order periodic attractor as discussed below.

In order to better compare the difference between boundaries of period-doubling and intermittency routes to chaos, we explicitly consider the two largest Lyapunov exponents $\lambda_{1,2}$ when the control parameter c is varied as $c \in [32, 39]$, $a = b = 0.245$, i.e., crossing the B_1 and B_2 regions of the main shrimp structure (Fig. 13). The system generates an inverse period-doubling route from chaos to periodic solutions, when the value c passes the inner boundary of the shrimp, i.e., $c \in (33.10, 35.07)$ in the B_1 region (Fig. 12). For further decreasing $c \in (32.72, 33.10)$, the system shows sparse chaos [highlighted by yellow background color in Fig. 13(b)]. We note that all three considered ordinal measures are blurred in this region of weak sparse chaos (Fig. 14). Note that sparse chaos resulting from a period-doubling route largely resembles the periodic attractor's geometry [compare the phase portraits in the subsets of Fig. 13(a)]. In contrast,

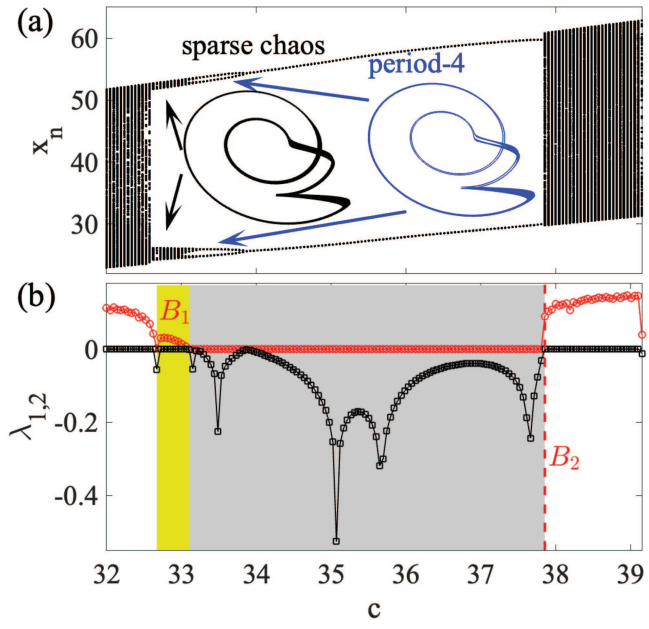

FIG. 13. Bifurcation diagram of the Rössler system when the control parameter c crosses boundaries of shrimps B_1 and B_2. (a) x_n on the Poincaré section $y = 0$, and (b) Lyapunov exponents $\lambda_{1,2}$, where the main periodic window is highlighted by gray background. The window of weak sparse chaos resulting from period-doubling is highlighted by light yellow color. Two typical phase portrait of sparse chaos and period-4 are, respectively, zoomed in the subsets of (a).

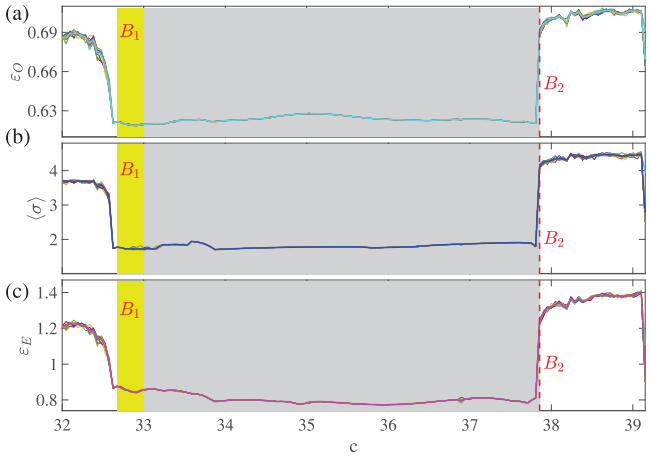

FIG. 14. One parameter bifurcation diagram of the Rössler system as characterized by ordinal measures. (a) ε_O, (b) $\langle\sigma\rangle$, and (c) ε_O.

all values of ordinal measures provide pronounced distinctions for the B_2 boundaries of intermittency to chaos (Fig. 14).

V. CONCLUSIONS

Different bifurcation scenarios associated with various boundaries of shrimp structures present an opportunity to design and test appropriate statistical measures for classifying the resulting dynamics. In this work, we demonstrate that the out-link transition entropy ε_E of OPTN shows fast convergence to stable values when using relatively short time series lengths and embedding dimension $D \sim 5$ or 6, comparable to the traditional static permutation entropy ε_O and averaged amplitude fluctuations of ordinal patterns $\langle\sigma\rangle$.

We find that the OPTN out-link transition entropy ε_E successfully characterizes different bifurcation routes to chaos, in particular, period-doubling and intermittency. Using the parameter space of the Rössler system as an illustrative example, we show that ε_E captures different dynamics, exhibiting a high classification accuracy for periodic and chaotic behavior. Under the supervision of the maximal Lyapunov exponents, we demonstrate that ε_E performs best in comparison to ε_O and $\langle\sigma\rangle$. To this end, a systematic comparison of our approach with other time series analysis methods, particularly such based on alternative complex network approaches, however remains a subject of future work.

In addition, it will be an interesting task to experimentally investigate shrimp structures, which is certainly helpful for dynamics control and navigation in parameter space. In such a practical case, we suggest that one should follow the traditional way of constructing ordinal patterns,[36,37] while considering the temporal transition frequencies between patterns.

ACKNOWLEDGMENTS

Parts of this work was financially supported by the National Natural Science Foundation of China (Grant Nos. 42461144209, 12272150, and 12072132), the STI2030-Major Projects (Grant No. 2021ZD0202600), and the Natural Science Foundation of Shanghai (Grant No. 24ZR1420700).

AUTHOR DECLARATIONS

Conflict of Interest

The authors have no conflicts to disclose.

Author Contributions

Yong Zou: Conceptualization (equal); Formal analysis (equal); Funding acquisition (equal); Investigation (equal); Methodology (equal); Writing – original draft (equal). **Norbert Marwan:** Formal analysis (supporting); Methodology (supporting); Writing – original draft (supporting); Writing – review & editing (supporting). **Xiujing Han:** Funding acquisition (supporting); Writing – review & editing (supporting). **Reik V. Donner:** Methodology (supporting); Writing – review & editing (supporting). **Jürgen Kurths:** Conceptualization (supporting); Methodology (supporting); Writing – original draft (supporting); Writing – review & editing (supporting).

DATA AVAILABILITY

The data that support the findings of this study are available within the article.

APPENDIX A: MISSING PATTERNS AND TRANSITIONS IN THE LOGISTIC MAP

In the example of the Rössler system (Fig. 1), we have shown that there are many missing ordinal patterns mainly due to the fact that consecutive increasing or decreasing sampling points are rare in continuous time series. However, we emphasize that the missing patterns are determined by the underlying dynamical process and also depend on the choice of embedding dimension D and delay τ. Here, we use the discrete case of the logistic map ($r = 4$) as another illustrative example, where missing patterns have been analytically

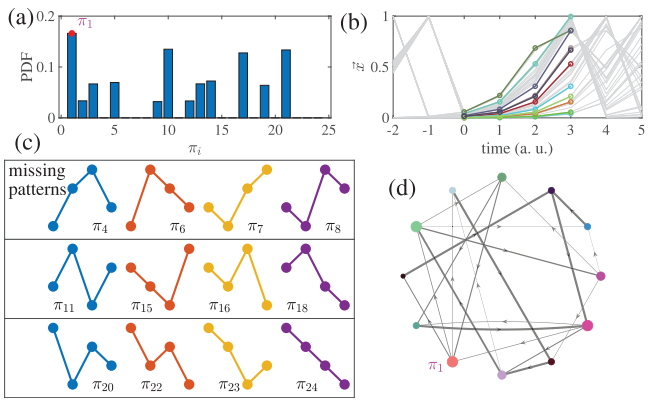

FIG. 15. Missing patterns and missing transitions in the logistic map $r = 4$. (a) Distribution of ordinal patterns. (b) Different embedding vectors sharing the same ordinal patterns. (c) Missing patterns. (d) Globally normalized transition matrix.

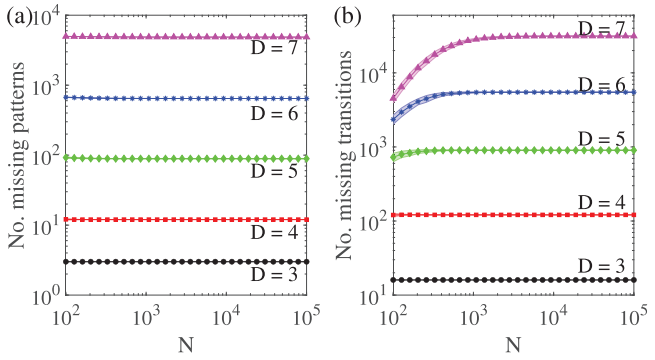

FIG. 16. Convergence of missing patterns and missing transitions in the logistic map with $r = 4$ for different dimensions $D \in \{3, \ldots, 7\}$. (a) Missing ordinal patterns. (b) Missing pattern transitions. The shaded areas for error bars are negligible in all cases.

calculated previously by Amigó *et al.*[49] for $\tau = 1$. They showed that the pattern $\pi = (2, 1, 0)$ never appears as well as the general pattern $\pi = (*, 2, *, 1, *, 0, *)$ where $*$ represents any other ranking, which is due to the fact that $f^2(x) < f(x) < x$ never happens, which, in turn, is termed a forbidden pattern. The appearance of forbidden patterns helps us design proper discriminators to distinguish chaos from noise.[15]

For the illustrative case of $D = 4$, we find that the consecutive increasing pattern π_1 has the largest appearance frequency [Fig. 15(a)]. In addition, there are many time series segments that share the same rank order of π_1 [Fig. 15(b)]. However, the patterns of consecutively decreasing values are largely missing [Fig. 15(c)]. In turn, a large number of missing pattern transitions are observed, which are suppressed from the visualization in Fig. 15(d). Note that the delay $\tau = 1$ is widely suggested for discrete time series. The results of Fig. 15 will change if different τ values are used.

In addition, we show the average number of missing patterns of dimension D that are found in a time series of length N, which is denoted as $\langle n(D, N) \rangle$. We find that $\langle n(D, N) \rangle$ converges quickly to stable values for all embedding dimensions $D \in \{3, \ldots, 7\}$ when the time series length $N \geq 10^2$ [Fig. 16(a)]. Rather similar results are observed for the number of missing transitions between different patterns [Fig. 16(b)]. The difference only appears when $N < 10^3$ for relatively large $D \in \{5, \ldots, 7\}$. In general, a time series length of $N < 10^3$ is not long enough to correctly identify all missing transitions, because the number of possible pattern transitions grows as $D! \times D!$.

APPENDIX B: BIFURCATION DIAGRAM OF THE POINCARÉ SECTION OF THE RÖSSLER SYSTEM

We finally employ a Poincaré section to sample the continuous time series of the x coordinate of the Rössler system at $y = 0$, $\dot{y} < 0$ and construct OPTNs from 10^4 intersection points. The three ordinal measures capture successfully the major periodic windows of the system, which are shown in Fig. 17. Specifically, for periodic windows, both $\langle \sigma \rangle$ and ε_O take values of zero, which reflects the completely deterministic nature of successions between a (low)

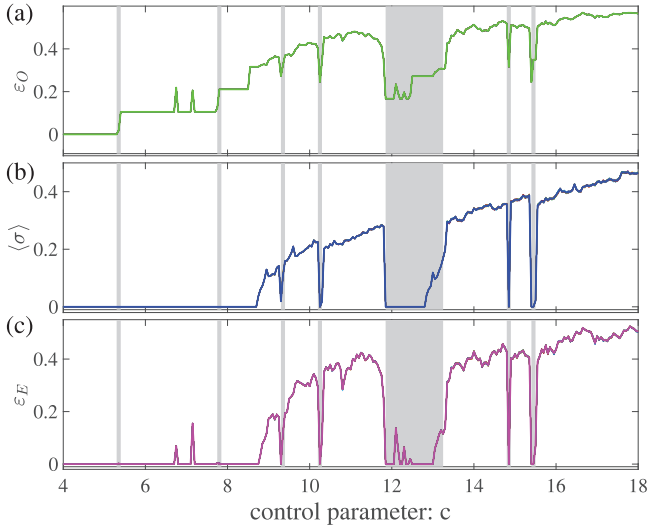

FIG. 17. Same as in Fig. 6, but based on the consecutive intersection points on the x coordinates of the Poincaré section $y = 0$ ($\dot{y} < 0$) of the Rössler system. (a) ε_O, (b) $\langle \sigma \rangle$, and (c) ε_O. Embedding dimension $D = 6$ and delay $\tau = 1$.

number of fixed intersection points in the Poincaré map that repeat always in exactly the same order.

REFERENCES

[1] J. Zhang and M. Small, Phys. Rev. Lett. **96**, 238701 (2006).
[2] L. Lacasa, B. Luque, F. Ballesteros, J. Luque, and J. C. Nuno, Proc. Natl. Acad. Sci. U.S.A. **105**, 4972 (2008).
[3] N. Marwan, J. F. Donges, Y. Zou, R. V. Donner, and J. Kurths, Phys. Lett. A **373**, 4246 (2009).
[4] R. V. Donner, Y. Zou, J. F. Donges, N. Marwan, and J. Kurths, New J. Phys. **12**, 033025 (2010).
[5] J. Y. Zhang, J. Zhou, M. Tang, H. Guo, M. Small, and Y. Zou, Sci. Rep. **7**, 7795 (2017).
[6] Y. Zou, R. V. Donner, N. Marwan, J. F. Donges, and J. Kurths, Phys. Rep. **787**, 1 (2019).
[7] J. S. A. E. Fouda, W. Koepf, N. Marwan, J. Kurths, and T. Penzel, Chaos, Solitons Fractals **181**, 114708 (2024).
[8] A. Nuñez, L. Lacasa, J. Patricio, and B. Luque, in *New Frontiers in Graph Theory* (InTech, 2012), Chap. 6, pp. 119–152.
[9] G. Nicolis, A. G. Cantu, and C. Nicolis, Int. J. Bifurcat. Chaos **15**, 3467 (2005).
[10] X. Xu, J. Zhang, and M. Small, Proc. Natl. Acad. Sci. U.S.A. **105**, 19601 (2008).
[11] M. McCullough, M. Small, T. Stemler, and H. H.-C. Iu, Chaos **25**, 053101 (2015).
[12] M. McCullough, M. Small, H. H. C. Iu, and T. Stemler, Philos. Trans. R. Soc. A Math. Phys. Eng. Sci. **375**, 20160292 (2017).
[13] H. Kantz and T. Schreiber, *Nonlinear Time Series Analysis*, 2nded. (Cambridge University Press, Cambridge, 2004).
[14] C. Bandt and B. Pompe, Phys. Rev. Lett. **88**, 174102 (2002).
[15] M. Zanin and F. Olivares, Commun. Phys. **4**, 190 (2021).
[16] Y. Hirata and J. M. Amigó, Chaos **33**, 052101 (2023).
[17] C. W. Kulp, J. M. Chobot, H. R. Freitas, and G. D. Sprechini, Chaos **26**, 073114 (2016).
[18] Y. Ruan, R. V. Donner, S. Guan, and Y. Zou, Chaos **29**, 043111 (2019).
[19] J. A. Almendral, I. Leyva, and I. Sendiña-Nadal, Entropy **25**, 1079 (2023).
[20] A. Politi, Phys. Rev. Lett. **118**, 144101 (2017).
[21] J. A. C. Gallas, Phys. Rev. Lett. **70**, 2714 (1993).

[22]J. A. C. Gallas, Phys. A **202**, 196 (1994).
[23]Y. Zou, M. Thiel, M. Romano, Q. Bi, and J. Kurths, Int. J. Bifurcat. Chaos Appl. Sci. Eng. **16**, 3567 (2006).
[24]C. Bonatto, J. Garreau, and J. Gallas, Phys. Rev. Lett. **95**, 143905 (2005).
[25]R. M. da Silva, N. S. Nicolau, C. Manchein, and M. W. Beims, Phys. Rev. E **98**, 032210 (2018).
[26]M. Mugnaine, M. R. Sales, J. D. Szezech, and R. L. Viana, Phys. Rev. E **106**, 034203 (2022).
[27]V. E. Camargo, A. S. Amaral, A. F. Crepaldi, and F. F. Ferreira, Chaos **32**, 103112 (2022).
[28]E. S. Medeiros, U. Feudel, and A. Zakharova, Phys. Rev. E **104**, 024302 (2021).
[29]J. A. C. Gallas and L. F. Olsen, Chaos **32**, 063122 (2022).
[30]E. L. Brugnago, E. C. Gabrick, K. C. Iarosz, J. D. Szezech, R. L. Viana, A. M. Batista, and I. L. Caldas, Chaos **33**, 123123 (2023).
[31]Á. G. López, R. Ali, L. Mandi, and P. Chatterjee, Chaos **31**, 013104 (2021).
[32]C. Bonatto and J. A. C. Gallas, Phys. Rev. Lett. **101**, 054101 (2008).
[33]R. Stoop, P. Benner, and Y. Uwate, Phys. Rev. Lett. **105**, 074102 (2010).
[34]C. Bonatto and J. Gallas, Phys. Rev. E **75**, 055204 (2007).
[35]E. Barreto, B. Hunt, C. Grebogi, and J. Yorke, Phys. Rev. Lett. **78**, 4561 (1997).
[36]J. M. Amigó, K. Keller, and V. A. Unakafova, Philos. Trans. R. Soc. A **373**, 20140091 (2014).
[37]J. M. Amigó and O. A. Rosso, Chaos **33**, 080401 (2023).
[38]F. Takens, in *Dynamical Systems and Turbulence, Warwick 1980*, Lecture Notes in Mathematics, Vol. 898, edited by D. Rand and L.-S. Young (Springer, New York, 1981), pp. 366–381.
[39]W. Yao, Phys. Rev. E **109**, 054104 (2024).
[40]O. A. Rosso, H. A. Larrondo, M. T. Martin, A. Plastino, and M. A. Fuentes, Phys. Rev. Lett. **99**, 154102 (2007).
[41]R. López-Ruiz, H. L. Mancini, and X. Calbet, Phys. Lett. A **209**, 321 (1995).
[42]A. M. Kowalski, M. T. Martin, A. Plastino, O. A. Rosso, and M. Casas, Entropy **13**, 1055 (2011).
[43]M. Huang, Z. Sun, R. V. Donner, J. Zhang, S. Guan, and Y. Zou, Chaos **31**, 033127 (2021).
[44]S. Zambrano, I. P. Mariño, and M. A. F. Sanjuán, New J. Phys. **11**, 023025 (2009).
[45]A. C. Fowler and M. J. Mcguinness, ANZIAM J. **65**, 93–110 (2023).
[46]Y. Zou, R. V. Donner, J. F. Donges, N. Marwan, and J. Kurths, Chaos **20**, 043130 (2010).
[47]M. Hollander and D. A. Wolfe, *Nonparametric Statistical Methods*, 2nded. (Wiley, New York, 1999).
[48]T. Fawcett, Pattern Recognit. Lett. **27**, 861 (2006).
[49]J. M. Amigó, S. Zambrano, and M. A. F. Sanjuán, Europhys. Lett. **79**, 50001 (2007).